

Real-time monitoring of surface processes by *p*-polarized reflectance

N. Dietz,^{a)} N. Sukidi, C. Harris, and K. J. Bachmann

Departments of Physics and Materials Science and Engineering, North Carolina State University, Raleigh, North Carolina 27696-7919

(Received 14 October 1996; accepted 11 March 1997)

Understanding surface chemistry under steady-state epitaxial growth involving organo-metallic chemical precursor molecules is essential for optimizing growth processes. Surface-sensitive optical real-time sensor techniques are very well suited for this task as their applications are not limited to a high vacuum environment. In this article we report the combined application of the optical sensor techniques *p*-polarized reflectance (PR) and laser light scattering for the real-time monitoring of low temperature growth of epitaxial GaP/Ga_xIn_{1-x}P heterostructures on Si(001) and GaAs(001) substrates by pulsed chemical beam epitaxy. The high surface sensitivity of PR allows to follow growth processes with submonolayer resolution during the sequential precursor exposure of the surface that causes periodic alterations in composition and thickness of a surface reaction layer (SRL), the effect of which is monitored by PR as a periodic fine structure. This fine structure is superimposed on interference oscillations, resulting from back reflection at the substrate-layer interface with increasing layer thickness. In a linear approximation of the complex four-layer stack reflectance amplitude RR_4 in the phase factor Φ_1 , the optical response to the SRL is formulated as an additive term in the three-layer model that describes the underlying film growth process. Analytical expressions for the first derivative of the PR signal are presented and discussed with respect to the time scale of observation that allows the separation of film growth induced changes from SRL effects. The amplitude modulation and the turning points in the fine structure are assessed and compared to experimental results, showing that an average complex dielectric function of an ultrathin SRL can be quantified, independent of surface coverage. © 1997 American Vacuum Society. [S0734-2101(97)08603-X]

I. INTRODUCTION

Research concerning the integration of polar compound semiconductors on nonpolar Si substrates is motivated by several decades of technological applications and it becomes even more important with regard to the advanced state of silicon technology. However, progress in understanding and control of the heteroepitaxial nucleation and overgrowth has been very slow, considering little is known about defect formation and interactions and propagation of defects during the later stages of compound heteroepitaxy on silicon. To gain a better understanding of the deposition process and the surface chemistry involved nonintrusive optical real-time process techniques have been developed and successfully applied during the last decade; these have focused on the monitoring of either bulk-film properties¹⁻⁴ or surface processes by reflection high energy electron diffraction (RHEED) or reflectance difference spectroscopy (RDS).⁵ For real-time close-loop deposition control, a product driven virtual substrate approach was recently introduced.⁶ For the monitoring of both bulk and surface, we have recently added *p*-polarized reflectance spectroscopy (PRS) and demonstrated its capability during pulsed chemical beam epitaxy (PCBE) of III-V heteroepitaxial growth.

II. EXPERIMENT

The *p*-polarized reflectance (PR) and laser light scattering (LLS) data are simultaneously obtained to monitor heteroepi-

taxial film growth under pulsed chemical beam epitaxy conditions. The surface of the substrate is exposed to pulsed ballistic beams of tertiarybutyl phosphine [TBP, (C₄H₉)PH₂], triethylgallium [TEG, Ga(C₂H₅)₃] and trimethylindium [TMI, In(CH₃)₃] at typically 350–400 °C to accomplish nucleation and overgrowth of silicon/GaAs substrates by an epitaxial GaInP film. The fluxes of the precursor and hydrogen are established by mass flow controllers and are directed via computer-controlled three-way valves to either the reactor chamber or a separately pumped bypass chamber. The switching of the sources is synchronized with the data acquisition of the PR and LLS signals in order to correlate the changes in the reflected intensity to the changes in the optical properties of the heteroepitaxial stack that encompass chemistry-induced changes in the surface composition and changes due to the thickness and optical properties of the epitaxial film. Typical growth rates under the chosen PCBE growth conditions are in the order of 1 Å/s, with TBP:TEG flux ratios in the range 30:1–40:1 and a constant hydrogen flux of 5 sccm in the background. The GaAs substrates are *ex situ* chemically etched in Br:methanol (0.02%) solution, follow by a DI-H₂O rinse, a NH₄OH:H₂O (1:1) dip and a final DI-H₂O rinse prior loading in the growth chamber. The substrates are then heated to 580 °C under H₂ (10⁻⁴ mTorr) atmosphere for 5 min. Growth is indicated upon lowering and stabilizing the substrate temperature to 400 °C. Further details on the experimental conditions are given in previous publications.⁷⁻¹⁴

^{a)}Electronic mail: dietz@mte.ncsu.edu

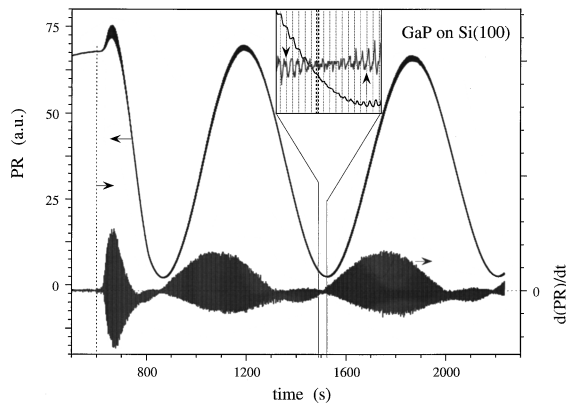


FIG. 1. PR and $d(PR)/dt$ evolution for heteroepitaxial GaP growth on Si under PCBE conditions at 350 °C. The inset shows an enlargement around a turning point, where the response to the first precursor (marked by arrows) changes sign. The start of each pulse cycle sequence in the inset is indicated by a dashed line, where the distance between each dash represents one pulse cycle sequence of 3 sec.

III. RESULTS AND SIMULATION OF THE SURFACE REACTION LAYER

Figure 1 shows the evolution of the PRS signal with its first derivative during the growth of GaP on Si(001) at 350 °C with a precursor cycle sequence time of 3 sec. The evolution of the PR signal during growth can be analyzed in terms of the bulk and surface properties of the film as is described elsewhere.¹⁵ The fine structure observed in the PR signal (see inset in Fig. 1) is strongly correlated to the time sequence of the supply of precursors employed during the steady-state growth of GaP. Each peak in the fine structure corresponds to a complete precursor cycle with the start of the oscillation always coinciding with the leading edge of the first TBP pulse of the sequence. As it can be seen in Fig. 1, the amplitude in the fine structure undergoes periodic changes during deposition time. The amplitude increases on the rising flank of the interference oscillation with a maximum at the top, and then decreases on the falling flank. The relative locations of these decreases and increases in the fine structure amplitude and the film interference oscillation strongly depend on the chosen growth conditions, such as precursor pulse width and height, pulse sequence time, or the supply of additional activated hydrogen. The inset shows that the reflectivity response to the first TBP precursor pulse in each cycle sequence changes from a rising transient (first arrow) to a falling transient (second arrow). This changeover in the sign with respect to the optical response of the first precursor pulse will hereafter be referred to as the turning point of the fine structure. This characteristic feature can be identified in the first derivative of the PR signal as the minima extreme, as shown in Fig. 1. The envelope function of $d(PR)/dt$ shows two important features.

(1) At the beginning of the heteroepitaxial growth process—after an incubation period of several precursor cycle sequences—a rapid increase in the $d(PR)/dt$ amplitude is observed.

(2) After the heteroepitaxial nucleation and overgrowth,

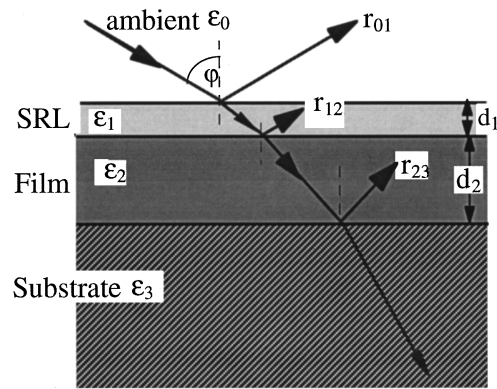


FIG. 2. Schematic representation of a four-layer stack.

the $d(PR)/dt$ evolution undergoes period oscillations, where one oscillation consists of a long period with a large amplitude and a short period with a small amplitude. The ratio of these periods and their amplitude strongly depend on the chosen precursor dose and exposure times. The minima extrema mark the position where the turning points of the fine structure occur. A more detailed analysis is given in Sec. IV of this article.

The deviation of the envelope function in $d(PR)/dt$ during the first 200 sec of heteroepitaxial growth indicates that the nucleation and overgrowth process may extend 60–70 cycle sequences before quasi-steady-state growth conditions are reached. This would confirm earlier reflectance difference (RD) observations which revealed an increase in the anisotropy during the first 100 sec of nucleation and overgrowth.¹⁶

IV. FINE STRUCTURE MODELING

The mathematical modeling of the fine structure superimposed to the interference oscillation of the PR signal was previously described under the simplified assumption of a periodically thickness modulated surface reaction layer (SRL) with an average dielectric function $\hat{\epsilon}_1$.¹³ Thereby, the changes in thickness were linked to the buildup of SRL with the thickness \hat{d}_1 by the first precursor pulse and the incorporation of the SRL in the underlying growing film after the second precursor pulse. With these assumptions the overall observed evolution of the PR signal is described, using Fresnel's equations and a four-layer (ambient/surface/layer/film/substrate) stack model as schematically shown in Fig. 2. In the following text, the average dielectric function will be denoted as $\hat{\epsilon}_1$, while an exact value for the dielectric function will be denoted as ϵ_1 . Similar, to this $d_1(t)$ describes the exact thickness and \hat{d}_1 the average thickness of the SRL. The distinction is of importance since the composition and therefore ϵ_1 changes during the pulsed exposure in a time scale of fractions of a sec. No data are presently available to describe the evolution of ϵ_1 in this time scale.¹⁶ The simulation by this simple model reveals two important features.

(1) There is a periodic amplitude modulation that is linked to interference oscillations, where the relative positions of

the minima in the fine structure amplitude with respect to the positions in the minima of the interference oscillations depend upon the differences in the dielectric functions of SRL and the underlying bulk.

(2) A change of sign to the response to first and second precursor pulses occurs at the minima of the fine structure amplitude, referred to as turning points. The location of these turning points with respect to the extreme of the interference oscillation is a measure of the imaginary part of the SRL dielectric function.

In a more detailed model the simplifications in the above model have to be corrected to account for changes in both the thickness and dielectric function of the SRL as the growth process progresses. This requires correlation of the structure in the PR intensity to the changing of defragmentation products and their concentrations in the surface reaction layer, which is discussed in more detail elsewhere.¹⁷

Fresnel's equations for a multilayer stack are used to calculate changes of the reflectivity for p -polarized light as a function of layer thickness, assuming homogeneous isotropic media. Numbering the media forming throughout the multilayer stack, starting with '0' for ambient, the reflectance coefficients $r_{k(k+1)}$ for the interfaces are given by¹⁸

$$r_{k(k+1)} = \frac{\varepsilon_{k+1} \cdot \sqrt{\varepsilon_k - \varepsilon_0 \sin^2 \varphi} - \varepsilon_k \cdot \sqrt{\varepsilon_{k+1} - \varepsilon_0 \sin^2 \varphi}}{\varepsilon_{k+1} \cdot \sqrt{\varepsilon_k - \varepsilon_0 \sin^2 \varphi} + \varepsilon_k \cdot \sqrt{\varepsilon_{k+1} - \varepsilon_0 \sin^2 \varphi}}, \quad (k \geq 0). \quad (1)$$

Here, in the four-layer stack model used, 0 denotes the ambient, 1 the surface reaction layer, 2 the film, and 3 the substrate, with their complex dielectric constants ε_0 , ε_1 , ε_2 , and ε_3 , respectively. The imaginary part of a complex variable will be denoted by $\text{Im}(\varepsilon)$ or ε^i and the real part by $\text{Re}(\varepsilon)$ or ε^r . The complex reflectance amplitude rr_4 for p -polarized light is given by¹⁸

$$rr_4 = \frac{r_{0,1} + r_{1,2} e^{-2j\Phi_1} + r_{2,3} e^{-2j(\Phi_1 + \Phi_2)} + r_{0,1} r_{1,2} r_{2,3} e^{-2j\Phi_2}}{1 + r_{0,1} r_{1,2} e^{-2j\Phi_1} + r_{0,1} r_{2,3} e^{-2j(\Phi_1 + \Phi_2)} + r_{1,2} r_{2,3} e^{-2j\Phi_2}}, \quad (2)$$

with the phase factors

$$R_3 = \frac{|r_{0,2}|^2 + |r_{2,3}|^2 e^{4y} + 2e^{2y} [r_{0,2}^r (r_{2,3}^r \cos 2x + r_{2,3}^i \sin 2x) + r_{0,2}^i (r_{2,3}^r \cos 2x - r_{2,3}^i \sin 2x)]}{1 + |r_{0,2}|^2 |r_{2,3}|^2 e^{4y} + 2e^{2y} [r_{0,2}^r (r_{2,3}^r \cos 2x + r_{2,3}^i \sin 2x) - r_{0,2}^i (r_{2,3}^r \cos 2x - r_{2,3}^i \sin 2x)]} \\ [x = \phi_2^r(\tilde{t}) \quad \text{and} \quad y = \phi_2^i(\tilde{t})], \quad (7)$$

where $r_{0,2}$ denotes the reflectance coefficient between ambient and film, neglecting the SRL. The first derivative of rr_4 in Φ_1 is given by the expression

$$\frac{\partial rr_4}{\partial \Phi_1} = \frac{-2je^{-2j\Phi_1}(1 - r_{0,1}^2)(r_{1,2} + r_{2,3}e^{-2j\Phi_2})(1 + r_{1,2}r_{2,3}e^{-2j\Phi_2})}{(1 + r_{0,1}r_{1,2}e^{-2j\Phi_1})^2 + 2\xi_1 r_{2,3}e^{-2j\Phi_2} + r_{2,3}^2(r_{1,2} + r_{0,1}e^{-2j\Phi_1})^2 e^{4j\Phi_2}}, \quad (8)$$

with $\xi_1 = r_{1,2} + r_{0,1}e^{-2j\Phi_1}(1 + r_{1,2}^2 + r_{0,1}r_{1,2}e^{-2j\Phi_1})$.

In the limit of $\Phi_1 = 0$, Eq. (8) reduces to

$$\Phi_1(t) = \frac{2\pi \hat{d}_1(t)}{\lambda} \sqrt{\hat{\varepsilon}_1(t) - \varepsilon_0 \sin^2 \varphi}, \quad (3)$$

and

$$\Phi_2(t) = \frac{2\pi d_2(t)}{\lambda} \sqrt{\varepsilon_2 - \varepsilon_0 \sin^2 \varphi}. \quad (4)$$

$d_1(t)$ and $d_2(t)$ are the thicknesses of the SRL and the film, respectively, λ is the wavelength of the reflected p -polarized laser beam and φ is the angle of incidence. Since only p -polarized light is considered in the following, the index p is dropped for simplification.

The reflectivity of the four-layer stack is given by $R_4 = rr_4 \cdot rr_4^*$, which can be approximated in a linear expansion for rr_4 in Φ_1 by

$$rr_4 \approx rr_4(\Phi_1 = 0) + \Phi_1 \cdot \left. \frac{\partial rr_4}{\partial \Phi_1} \right|_{\Phi_1 = 0} = rr_3 + rr_{4\alpha} \cdot \Phi_1. \quad (5)$$

With this, the reflectivity in a four-layer stack is given by

$$R_4|_{ap} \approx rr_3 \cdot rr_3^* + rr_3 \Phi_1^* rr_{4\alpha}^* + rr_3^* \Phi_1 rr_{4\alpha} \\ + |\Phi_1|^2 |rr_{4\alpha}|^2 \\ = R_3 + 2 \text{Re}\{rr_3^* \Phi_1 rr_{4\alpha}\} + |\Phi_1|^2 |rr_{4\alpha}|^2 \\ = R_3 + \Delta R_{4,3}, \quad (6)$$

where R_3 denotes the reflectivity for the three-layer stack (without SRL), $\Delta R_{4,3}$ the linear approximation of the SRL contribution and $rr_{4\alpha}$ the derivative of the complex reflectance amplitude rr_4 in Φ_1 at $\Phi_1 = 0$.

The reflectivity, $R_3 = rr_3 \cdot rr_3^*$, is given by

$$\left. \frac{\partial r r_4}{\partial \Phi_1} \right|_{\Phi_1=0} = \frac{-2j(1-r_{0,2}^2)r_{2,3}e^{-2j\Phi_2}}{(1+r_{0,2}r_{2,3}e^{-2j\Phi_2})^2}, \quad (9)$$

taking in account that $\Phi_1 \rightarrow 0$ implies $d_1 \rightarrow 0$ (for $\varepsilon_0 \approx 1$) and therefore $\varepsilon_1 \rightarrow \varepsilon_2$, which leads to $r_{1,2} \rightarrow 0$ and $r_{0,1} \rightarrow r_{0,2}$ in the limit of $\Phi_1=0$. However, in a linear approximation of R_4 for small d_1 , the transition of $\varepsilon_1 \rightarrow \varepsilon_2$ is not valid and the reflection coefficients $r_{1,2}$ and $r_{0,1}$ still have to be considered. Leaving these terms, $r r_{4\alpha}$ can be written as

$$r r_{4\alpha} = \frac{-2j(1-r_{0,1}^2)(r_{1,2}+r_{2,3}e^{-2j\Phi_2})(1+r_{1,2}r_{2,3}e^{-2j\Phi_2})}{(1+r_{0,1}r_{1,2})^2+2r_{2,3}e^{-2j\Phi_2}[r_{1,2}+r_{0,1}(1+r_{1,2}^2+r_{0,1}r_{1,2})]+r_{2,3}^2(r_{0,1}+r_{1,2})^2e^{-4j\Phi_2}}. \quad (10)$$

In the analysis of the timely evolution of the fine structure which is superimposed with the interference oscillations of the underlying growing film, the different time evolution of the both phase factors Φ_1 and Φ_2 can be utilized to separate contributions related to the SRL and thus related to the bulk film. Assuming time dependencies in $d_2(t)$, $d_1(t)$ and $\varepsilon_1(t)$, the derivative of R_4 in time is given by

$$\begin{aligned} \frac{dR_4}{dt} &= \frac{\partial R_4}{\partial \phi_2} \cdot \frac{\partial(\phi_2)}{\partial t} + \frac{\partial R_4}{\partial \phi_1} \cdot \frac{\partial(\phi_1)}{\partial t} + \left[\frac{\partial R_4}{\partial r_{1,2}} \cdot \frac{\partial r_{1,2}}{\partial \varepsilon_1} + \frac{\partial R_4}{\partial r_{0,1}} \cdot \frac{\partial r_{0,1}}{\partial \varepsilon_1} \right] \cdot \frac{\partial(\varepsilon_1)}{\partial t} \\ &\approx \frac{\partial R_3(t)}{\partial t} + \left[\frac{\partial[\Delta R_{4-3}]}{\partial \phi_1} \cdot \frac{\partial \phi_1}{\partial d_1} \right] \cdot \frac{\partial[d_1(t)]}{\partial t} + \left[\frac{\partial[\Delta R_{4-3}]}{\partial r_{1,2}} \cdot \frac{\partial r_{1,2}}{\partial \varepsilon_1} + \frac{\partial[\Delta R_{4-3}]}{\partial r_{0,1}} \cdot \frac{\partial r_{0,1}}{\partial \varepsilon_1} + \frac{\partial[\Delta R_{4-3}]}{\partial \phi_1} \cdot \frac{\partial \phi_1}{\partial \varepsilon_1} \right] \cdot \frac{\partial[\varepsilon_1(t)]}{\partial t}, \quad (11) \end{aligned}$$

where t denotes the time. dR_3/dt follows changes in $\phi_2(t)$ and is given by time dependence of the growing film $d_2(t)$, whereas the second term follows the temporal evolution of $d_1(t)$ and $\varepsilon_1(t)$ both varying due to the periodic precursor exposure of the surface, causing cyclic changes in thickness and composition in the SRL, expressed in the boundary condition

$$\Phi_1(t) = \Phi_1(t + T_{CS}) \quad (12)$$

under steady-state growth conditions.

The cycle sequence time T_{CS} is the order of a few seconds with precursor exposure times of tens of a second. Since the variation in time for both terms differs by more than a factor of 100, we can assume for small time interval ($t \leq 3s$) the timely changes in R_3 as linear.

The changes in R_3 as a function of $d_2(t)$ are expressed in

$$\frac{\partial R_3}{\partial t} = \frac{4e^{2y} \cdot (\chi_1 \operatorname{Im}[\tilde{\phi}_2] + \chi_2 \operatorname{Re}[\tilde{\phi}_2]) \cdot \partial(d_2)/\partial \tilde{t}}{(1+|r_{0,2}|^2|r_{2,3}|^2e^{4y} + 2e^{2y}[r_{0,2}^r(r_{2,3}^r \cos 2x + r_{2,3}^i \sin 2x) - r_{0,2}^i(r_{2,3}^i \cos 2x - r_{2,3}^r \sin 2x)])^2}, \quad (13)$$

with

$$\begin{aligned} \chi_1 &= |r_{2,3}|^2 e^{2y} [1 - |r_{0,2}|^4 + e^{2y} [r_{0,2}^r (r_{2,3}^r \cos 2x + r_{2,3}^i \sin 2x) - r_{0,2}^i (r_{2,3}^i \cos 2x - r_{2,3}^r \sin 2x)]] + (1 - |r_{0,2}|^2 |r_{2,3}|^2 e^{4y}) \\ &\quad \times [r_{0,2}^r (r_{2,3}^r \cos 2x + r_{2,3}^i \sin 2x) + r_{0,2}^i (r_{2,3}^i \cos 2x - r_{2,3}^r \sin 2x)], \end{aligned}$$

$$\begin{aligned} \chi_2 &= r_{0,2}^r (1 - |r_{0,2}|^2) (r_{2,3}^i \cos 2x - r_{2,3}^r \sin 2x) - r_{0,2}^i (1 + |r_{0,2}|^2) (r_{2,3}^r \cos 2x + r_{2,3}^i \sin 2x) \\ &\quad + |r_{2,3}|^2 e^{4y} [r_{0,2}^r (r_{2,3}^r \cos 2x + r_{2,3}^i \sin 2x) + r_{0,2}^i (r_{2,3}^i \cos 2x - r_{2,3}^r \sin 2x)] - 4e^{2y} r_{0,2}^r r_{0,2}^i |r_{2,3}|^2, \end{aligned}$$

$$\tilde{\phi}_2 = \frac{2\pi}{\lambda} \sqrt{\varepsilon_2 - \varepsilon_0} \sin^2 \varphi \quad x = \phi_2^r(\tilde{t}) \quad \text{and} \quad y = \phi_2^i(\tilde{t}),$$

which does not at this point include any changes due to a variation in composition $\varepsilon_2(t)$, which may have to be added if the layer with a graded composition is under consideration. $\partial R_3/\partial t$ varies slowly as the film thickness increases/decreases during a growing/etching process with time periods of several of hundred of seconds for the processes considered herein. For a transparent film with $r_{0,2}^i=0$ and $\partial \phi_2^i(t)/\partial t=0$, Eq. (12) simplifies to

$$\frac{\partial R_3}{\partial t} = \frac{4r_{0,2}^r (1 - |r_{0,2}|^2) (1 + |r_{2,3}|^2) (r_{2,3}^i \cos 2x - r_{2,3}^r \sin 2x)}{(1 + |r_{0,2}|^2 |r_{2,3}|^2 + 2r_{0,2}^r (r_{2,3}^r \cos 2x + r_{2,3}^i \sin 2x))^2} \cdot \operatorname{Re}\{\tilde{\phi}_2\} \frac{\partial d_2(t)}{\partial t}, \quad (14)$$

the properties of which are discussed in more detail elsewhere.¹⁷

The following modeling of the SRL induced fine structure in the reflectivity R_4 focuses on the difference in the reflectivities with and without the SRL contribution, which is given by

$$R_4 - R_3 \approx \Delta R_{4-3} = 2 \operatorname{Re}\{rr_3^* \Phi_1 rr_{4\alpha}\} + |\Phi_1|^2 |rr_{4\alpha}|^2, \quad (15)$$

and on its time dependency that is expressed in

$$\frac{\partial(\Delta R_{4-3})}{\partial t} \approx \left[\frac{\partial \Delta R_{4-3}}{\partial \phi_1} \frac{\partial \phi_1}{\partial d_1} \right] \frac{dd_1}{dt} + \left[\frac{\partial \Delta R_{4-3}}{\partial r_{1,2}} \frac{\partial r_{1,2}}{\partial \varepsilon_1} + \frac{\partial \Delta R_{4-3}}{\partial r_{0,1}} \frac{\partial r_{0,1}}{\partial \varepsilon_1} + \frac{\partial \Delta R_{4-3}}{\partial \phi_1} \frac{\partial \phi_1}{\partial \varepsilon_1} \right] \frac{\partial \varepsilon_1}{\partial t} + \left[\frac{\partial \Delta R_{4-3}}{\partial \phi_2} \frac{\partial \phi_2}{\partial d_2} \right] \frac{dd_2}{dt}. \quad (16)$$

Since at this time no sufficient data for the separation of $d_1(t)$ and $\varepsilon_1(t)$ are available, the simulations of the SRL induced fine structure are performed under a simplification that the variation in the phase factor $\Phi_1(t)$, caused either by $d_1(t)$ or $\varepsilon_1(t)$, can be described by a period changed $\Phi_1(t)$, using exponential build-up and decay functions as described previously.¹³ The increase in the layer thickness of the underlying growing film is assumed to be linear with time. A more detailed formulation of the decomposition process with corresponding changes in the dielectric function, $\varepsilon_1(t)$, and the time dependency of $d_1(t)$ in the SLR is given elsewhere.¹⁶

For all simulations shown below the following parameters were kept constant, unless indicated otherwise: complex dielectric function for the substrate of $\varepsilon_{\text{Si}} = 15.25 - i 0.17$,¹⁹ complex dielectric function for the bulk film of $\varepsilon_{\text{GaP}} = 11.0 - i 0.0$,²⁰ angle of incidence $\varphi = 72$ deg, wavelength $\lambda = 6328$ Å, cycle sequence 3 sec, with a TBP pulse from 0 to 0.8 sec, a TEG pulse from 1.4 to 1.8 sec and a growth rate 1 Å/s.

Figure 3 shows simulated reflectivity for a four-layer stack built up by the Si substrate, the growing GaP film with an average growth rate of 1 Å/sec, a periodic modulated SRL¹³ with $\varepsilon_1(\lambda = 632.8 \text{ nm}) = (9.5, 2.5)$ a minimal thickness of $d_{1 \min} = 0.5$ Å ($\rightarrow \phi_{1 \min}$) and maximal thickness of $d_{1 \max} = 5$ Å ($\rightarrow \phi_{1 \max}$), and an ambient with $\varepsilon_0 = 1$. The data for the dielectric function of the SRL are chosen such that they match the experimentally observed PR evolution shown in Fig. 1. Also shown are the calculated changes of $[R_4(t) - R_4(\phi_{1 \min})]$, the linear approximation ΔR_{4-3} (Eq. 15), the first derivatives of the three-layer stack $\partial R_3 / \partial t$ (Eq. 13), the four-layer stack $\partial R_4(t) / \partial t$ (Eq. 11) and its linear approximation $\partial(\Delta R_{4-3}) / \partial t$ (Eq. 16). A comparison of the results of our simulated spectra with the experimental results shows that under the specific growth conditions used in Fig. 1, the $\operatorname{Re}(\varepsilon_1)$ is smaller than $\operatorname{Re}(\varepsilon_2)$ with a significant absorption of $\operatorname{Im}(\varepsilon_1) = 2.5$. The fine structure evolution, not resolved in Fig. 3, is shown in more detail around the first and second turning points in Fig. 4.

Please note the following important features.

(1) The turning points are characterized by the condition

$$\{R_4[\phi_{1 \max}] - R_4(\phi_{1 \min})\} = 0. \quad (17)$$

(2) The error in the approximation of ΔR_{4-3} as a linear expansion of rr_4 in $\phi_1(t)$ is below 1 and describes very well the evolution of the PR signal. This is also valid for the

description of the first derivative of the PR signal. To attain this accuracy, $\phi_1(t)$ has to be carried with as a quadratic term in the calculated reflectance $\Delta R_{3-4}(t)$.

(3) The first derivative of dR_4/dt (second curve from the top in Fig. 4) can be decomposed in $\partial R_3 / \partial t$ and $\partial(\Delta R_{4-3}) / \partial t$ (top curve).

Under the limitations of this simulation the growth rate of the underlying film is assumed constant. Therefore, the simulated spectra do not contain a fine structure in $\partial R_3 / \partial t$. This assumption may have to be modified as more experimental data become available. This is especially true in the initial heteroepitaxial nucleation and growth period deviations in composition and thickness of the SRL that might be encountered compared to that during steady-state growth conditions.

To evaluate the sensitivity with which the average dielectric function ε_1 can be extracted, the complete parameter space of $\operatorname{Re}(\varepsilon_1)$ and $\operatorname{Im}(\varepsilon_1)$ has to be evaluated. Figure 5 shows the shift of the turning points as a function of

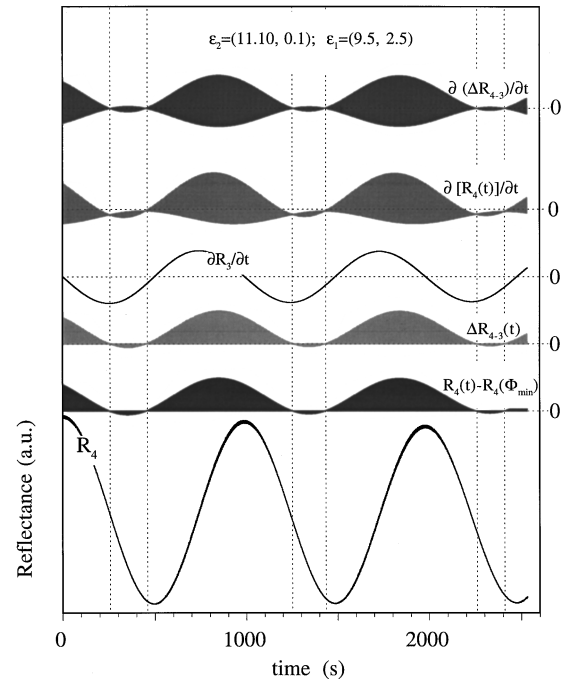


FIG. 3. Simulation of the temporal evolution of the PR signal in a four-layer stack model. The dashed lines mark the positions of the turning points. Also shown are the first derivative of the PR signal and contributions related to the SRL (see the text).

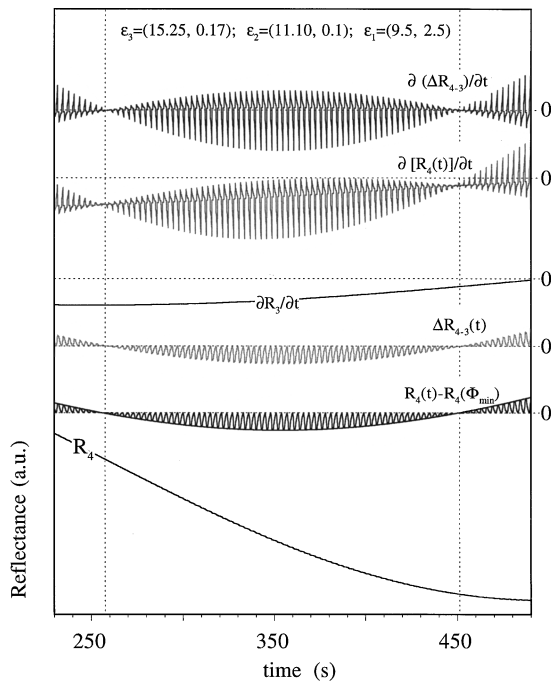


FIG. 4. PR signal and time evolution of the PR signal in the vicinity of the turning points (marked by dashed lines).

$\text{Re}(\epsilon_1)$ leaving $\text{Im}(\epsilon_1)=2$ constant. The turning points located at the increasing flank of the interference oscillation $\text{Re}(\epsilon_1)=6$ (lowest curve) are shifted to the left towards the falling flank of the interference oscillation for $\text{Re}(\epsilon_1)=6$ (top curve). For intermediate values of $\text{Re}(\epsilon_1)$ in the range of

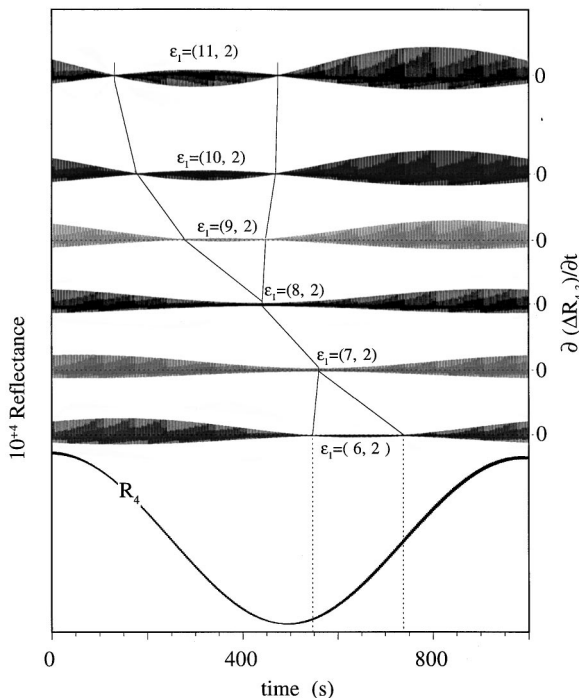


FIG. 5. Change of turning point positions (marked by dashed lines) relative to the interference extreme as a function of $\text{Re}(\epsilon_1)$.

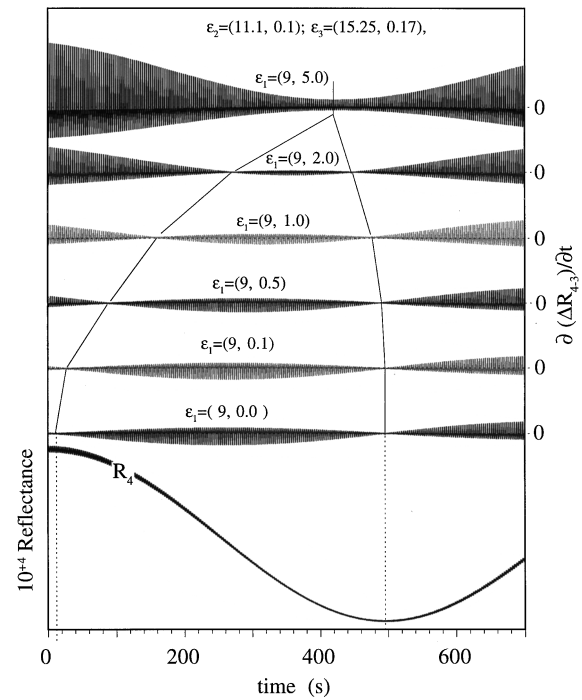


FIG. 6. Shift of the turning point positions (marked by dashed lines) along the falling flank of the interference oscillation with increasing absorption the SRL for $\text{Re}(\epsilon_1)=9$.

6.9–8.9 only a local minimum and no turning points are observed, which is due to the fact that $R_4[\phi_{1 \max}]$ is always larger $R_4[\phi_{1 \min}]$.

The contribution of the imaginary part to the position of the turning points is demonstrated in Figs. 6 and 7, which show the shift in the turning points as a function of absorption for two values of $\text{Re}(\epsilon_1)$. In Fig. 6 the turning points are located at the falling flank of the interference oscillation. With no absorption in the SRL, the position of the turning points coincides with the extreme of the interference oscillations. With increasing absorption $\text{Im}(\epsilon_1) > 0$, the turning points are close together, shifted downwards along the falling flank of the interference oscillation until for $\text{Im}(\epsilon_1) > 3$ only a local minimum remains. For $\text{Re}(\epsilon_1)$ values smaller than 7 for the same effect is observed in the rising flank of the interference oscillation as demonstrated for $\text{Re}(\epsilon_1)=6$ in Fig. 7.

The influence of the surface reaction layer thickness, d_1 is shown in Fig. 8, where the maximal thickness is varied from 2 Å up to 10 Å. As can be seen, a variation in the thickness of the SRL has no influence on the position of the turning points relative to the interference oscillation. An increase/decrease in the thickness of the SRL affects only the amplitude of the observed fine structure or its derivative. This phenomenon is due to the fact that the locations of the turning points are characterized by the values of the reflectance coefficients $r_{0,1}$, $r_{1,2}$, and $r_{2,3}$ as described by Eq. (1), which do not depend on the thickness d_1 . However, the amplitude of the PR signal is a function of the phase factors $\phi_1(t)$ and $\phi_2(t)$ and therefore affected by the variation of the thickness of the SRL.

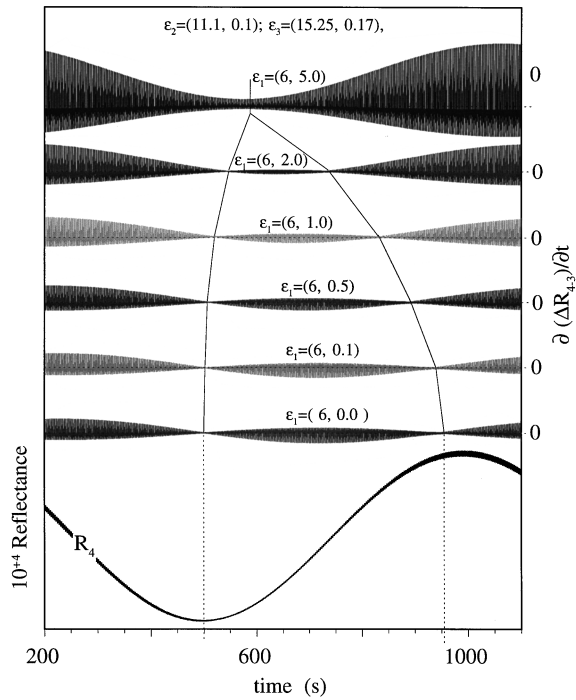


FIG. 7. Shift of the turning point positions (marked by dashed lines) along the rising flank of the interference oscillation with increasing absorption of the SRL for $\text{Re}(\epsilon_1)=6$.

Utilizing these features allows the extraction of the average dielectric function of the SRL, ϵ_1 , from the turning point locations which are independent to the surface coverage. Once ϵ_1 is computed, the amplitude of the fine structure

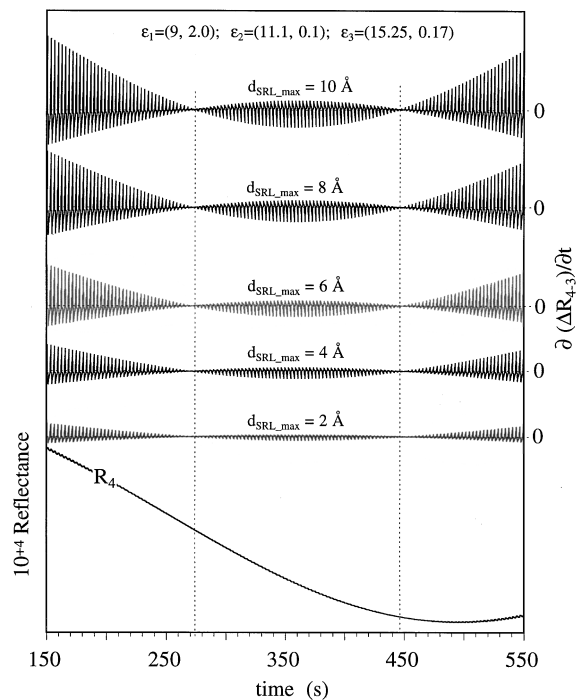


FIG. 8. Influence of surface coverage at the point positions relative to the interference extreme and the amplitude of the signal.

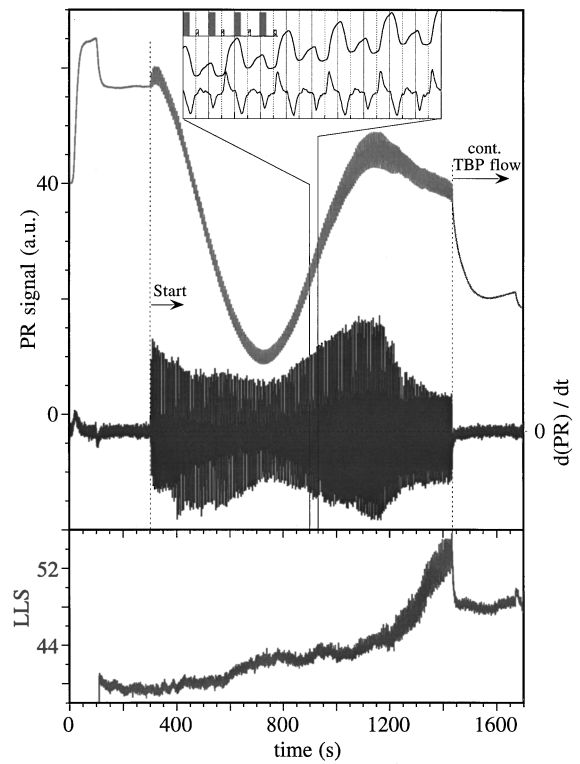


FIG. 9. PR, LLS, and $d(PR)/dT$ evolution during GaInP growth on a GaAs substrate at 400 °C.

and/or its derivative can be used in the next step to calculate the average surface coverage for the SRL.

V. CHARACTERIZATION OF SURFACE PROCESSES

Figure 9 shows the temporal evolution of the PRS and LLS signals during the growth of $\text{Ga}_x\text{In}_{1-x}\text{P}$ on GaAs(001). The flow ratio of TMI:TEG was set nominally to 1:1 with a TEG:TBP ratio of 1:40. The cycle sequence time is 6 sec, where the surface is sequentially exposed to two TBP pulses from 0.0 to 0.8 sec and 3.0 to 3.8 sec, one TEG pulse from 1.5 to 1.8 sec and one TMI pulse from 4.5 to 4.8 sec. Also shown (lower curve) is the evolution of the LLS intensity during the deposition process and the derivative, $dR_4(t)/dt$, of the PR signal. The response to sequential precursor exposure is shown enlarged in the inset of Fig. 9 (upper curve) together with its first derivative (lower curve). Upon initiating the growth, the PR signal shows an interference oscillation due to the increasing thickness of the film. Superimposed is a fine structure as a response to the pulsed precursor conditions. As indicated in the inset, the fine structure amplitude differs for the TEG and TMI exposure due to their different compositions and/or concentrations on the surface. After about 500 Å of film growth, the amplitude of the fine structure steadily increases reaching a maximum around 880 sec of growth and decreases rapidly afterwards. The increase in the fine structure amplitude might be explained as an accumulation of TMI fragments in the SRL until a critical supersaturation is reached at which a further accumulation

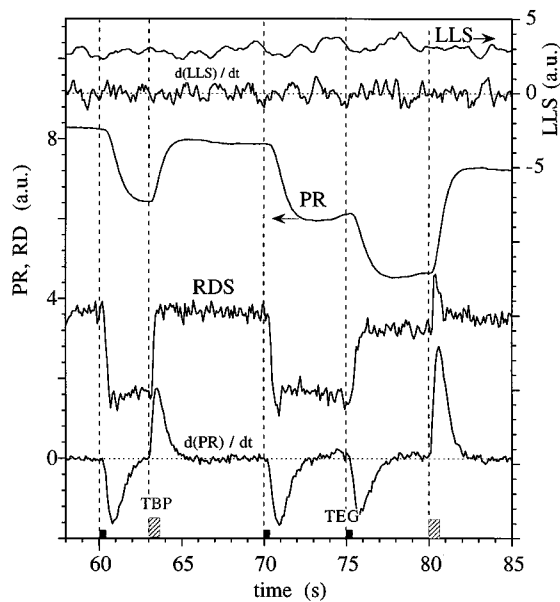


FIG. 10. PR, RD, and LLS responses for single TEG and TBP pulses of 0.5 sec in length monitored during an interruption of GaP growth at 350 °C on the falling edge of the PR interference oscillation (see the text). The first derivative of the PR signal coincides with the response times to the precursor exposure of the surface as detected by RD spectroscopy (see the text).

can no longer be accommodated, resulting in a spontaneous nucleation and three-dimensional (3D) growth. The breakdown in the SRL and the start of 3D growth is also characterized by a rapid increase in the surface roughening as observed in the LLS signal. After the termination of the $\text{Ga}_x\text{In}_{1-x}\text{P}$ growth, leaving continuous TBP flowing, the PRS signal as well as the LLS signal decreases, indicating a smoothing of the surface upon TBP exposure. At this time no information is available as to which precursor, TEG or TMI, has been accumulated in the SRL and has dominated the reactions kinetics. Even though PR is able to characterize the average evolution of the SRL, molecule specific spectroscopic techniques are required in conjunction with analysis of the transients in the fine structure to identify specific precursor fragments accumulated in the SRL.

For a more detailed understanding of surface reaction kinetics, experiments involving single pulses of TEG and TBP are performed under quasi-steady-state GaP growth conditions during growth interruptions of 100 sec. Figure 10 shows the PR, RD, and LLS transients during a series of individual pulses of TEG and TBP precursors, observed on a rising flank of the underlying PR interference oscillation at 350 °C with a continuous flow of molecular hydrogen present. The TBP and TEG fluxes are 0.8 sccm and 0.02 sccm, respectively. PR and LLS are monitored at 1.96 eV (HeNe laser) and RD spectroscopy at 2.6 eV.¹⁴ With the rising edge of TEG pulse the RD signal decreases linearly and shows an exponential decay after TEG exposure. The PR signal increases with a slight delay upon TEG exposure and the following TBP pulse resets the PR signal, except for a small shift due to the increased GaP layer thickness. However, the first derivative of the PR signal coincides with the

RD response time. Upon TEG exposure the RD and $d(\text{PR})/dt$ signals decrease linearly. The RD signal reaches a saturation level, whereas the $d(\text{PR})/dt$ signal returns to zero. During TBP exposure the $d(\text{PR})/dt$ signal increases immediately upon exposure while the RD signal is slightly delayed by 0.2 sec. The time dependence for the RD and $d(\text{PR})/dt$ signals is nearly identical, suggesting that the first derivative of the PR signal reveals similar features to RD.

VI. SUMMARY AND CONCLUSION

The real-time optical monitoring by p-polarized reflectance in combination with laser light scattering is demonstrated as a powerful tool to characterize growth processes as well as the surface chemistry under pulsed chemical beam growth conditions. Using a linear expansion for the complex four-layer stack reflectance amplitude rr_4 with respect to the phase factor Φ_1 , the optical response to the SRL can be written as an additive term in the three-layer model that describes the underlying film growth process. Analytical expressions for the first derivative of the PR signal were presented and discussed in order to obtain detailed information about the surface chemistry of the surface reaction layer. The amplitude modulation in the fine structure is analyzed and compared to experimental results. It was shown that the average complex dielectric function of an ultrathin SRL can be computed without being affected by the thickness of the surface reaction layer. For GaP growth with 3 sec pulse cycle time, an average dielectric function of $\epsilon_1=(9.5, 2.5)$ with an average thickness of 5 Å for the SRL was found to match experimental observations. The deviation of the envelope function in $d(\text{PR})/dt$ during the first 200 sec of heteroepitaxial growth indicates that the nucleation and overgrowth period extends to at least 60–70 cycle sequences.

ACKNOWLEDGMENTS

This work was supported by NSF Grant No. CDR 8721505, DOD-MURI Grant No. F49620-95-1-0447 and NASA Cooperative Agreement No. NCC8-95.

- ¹W. G. Breiland and K. P. Killeen, in Proceedings of the Material Research Society, Boston, MA, 29 Nov.–2 Dec. 1995, edited by O. J. P. Glembocki, S. W. Pollak, F. H. Crean, and G. M. Larrabee, p. 99.
- ²W. G. Breiland and K. P. Killeen, *J. Appl. Phys.* **78**, 6726 (1995).
- ³K. P. Killeen and W. G. Breiland, *J. Electron. Mater.* **23**, 179 (1993).
- ⁴S. D. Murthy, I. B. Bhat, B. Johs, S. Pittal, and P. He, *J. Electron. Mater.* **24**, 445 (1995).
- ⁵D. E. Aspnes, J. P. Harbison, A. A. Studna, and L. T. Florez, *Appl. Phys. Lett.* **52**, 957 (1988).
- ⁶D. E. Aspnes, *IEEE J. Sel. Topics Quantum Electron.* **1**, 1054 (1995).
- ⁷N. Dietz, A. Miller, J. T. Kelliher, D. Venables, and K. J. Bachmann, *J. Cryst. Growth* **150**, 691 (1995).
- ⁸N. Dietz, A. Miller, and K. J. Bachmann, *J. Vac. Sci. Technol. A* **13**, 153 (1995).
- ⁹K. J. Bachmann, U. Rossow, and N. Dietz, *Mater. Sci. Eng. B* **37**, 472 (1995).
- ¹⁰N. Dietz and K. J. Bachmann, *MRS Bull.* **20**, 49 (1995).
- ¹¹N. Dietz, U. Rossow, D. Aspnes, and K. J. Bachmann, *J. Electron. Mater.* **24**, 1571 (1995).
- ¹²K. J. Bachmann, N. Dietz, A. E. Miller, D. Venables, and J. T. Kelliher, *J. Vac. Sci. Technol. A* **13**, 696 (1995).
- ¹³N. Dietz and K. J. Bachmann, *Vacuum* **47**, 133 (1996).

- ¹⁴U. Rossow, N. Dietz, K. J. Bachmann, and D. E. Aspnes, *J. Vac. Sci. Technol. B* **14**, 3040 (1996).
- ¹⁵K. J. Bachmann, U. Rossow, N. Sukidi, H. Castleberry, and N. Dietz, *J. Vac. Sci. Technol. B* **14**, 3019 (1996).
- ¹⁶N. Dietz, U. Rossow, D. E. Aspnes, and K. J. Bachmann, *Appl. Surf. Sci.* **102**, 47 (1996).
- ¹⁷K. J. Bachmann, N. Sukidi, N. Dietz, C. Hoepfner, S. LeSure, H.T. Tran, S. Beeler, K. Ito, and H.T. Banks, *J. Cryst. Growth* (in press).
- ¹⁸N. Dietz, D. J. Stephens, G. Lucovsky, and K. J. Bachmann, *Mater. Res. Soc. Symp. Proc.* **324**, 27 (1994).
- ¹⁹D. F. Edwards, in *Handbook of Optical Constants*, edited by E. D. Palik (Academic, New York, 1985), p. 547.
- ²⁰A. Borghesi and G. Guizzetti, in Ref. 19, p. 445.